Degenerate four wave mixing in large mode area hybrid photonic crystal fibers

Petersen, Sidsel Rübner; Alkeskjold, Thomas Tanggaard; Lægsgaard, Jesper

Published in:
Optics Express

Link to article, DOI:
10.1364/OE.21.018111

Publication date:
2013

Document Version
Publisher's PDF, also known as Version of record

Degenerate four wave mixing in large mode area hybrid photonic crystal fibers

Sidsel R. Petersen,[1,*] **Thomas T. Alkeskjold,**[2] **and Jesper Lægsgaard**[1]

[1]*DTU Fotonik, Department of Photonics Engineering, Technical University of Denmark, Ørsteds Plads Building 343, 2800 Kgs. Lyngby, Denmark*
[2]*NKT Photonics A/S, Blokken 84, 3460 Birkerød, Denmark*
[*]*srpe@fotonik.dtu.dk*

Abstract: Spontaneous degenerate four wave mixing (FWM) is investigated in large mode area hybrid photonic crystal fibers, in which photonic bandgap guidance and index guidance is combined. Calculations show the parametric gain is maximum on the edge of a photonic bandgap, for a large range of pump wavelengths. The FWM products are observed on the edges of a transmission band experimentally, in good agreement with the numerical results. Thereby the bandedges can be used to control the spectral positions of FWM products through a proper fiber design. The parametric gain control combined with a large mode area fiber design potentially allows for power scaling of light at wavelengths not easily accessible with e.g. rare earth ions.

OCIS codes: (060.5295) Photonic crystal fibers; (060.4370) Nonlinear optics, fibers.

References and links

1. J. C. Knight, J. Arriaga, T. A. Birks, A. Ortigosa-Blanch, W. J. Wadsworth, and P. St. J. Russell "Anomalous Dispersion in Photonic Crystal Fiber," IEEE Photon. Technol. Lett. **12**(7), 807–809 (2000).
2. C. Jauregui, A. Steinmetz, J. Limpert, and A. Tünnermann, "High-power efficient generation of visible and mid-infrared radiation exploiting four-wave-mixing in optical fibers ," Opt. Express **20**(22), 24957–24965 (2012).
3. L. S. Rishøj, P. E. Steinvurzel, Y. Chen, L. Yan, J. D. Demas, M. D. W. Grogan, T. Ellenbogen, K. Crozier, K. Rottwitt and S. Ramachandran "High-Energy Four-Wave Mixing, with Large-Mode-Area Higher-Order Modes in Optical Fibres," ECOC Technical Digest, 38th European Conference and Exhibition on Optical Communication (2012).
4. T. T. Alkeskjold, "Large-mode-area ytterbium-doped fiber amplifier with distributed narrow spectral filtering and reduced bend sensitivity," Opt. Express **17**(19), 16394–16405 (2009).
5. S. R. Petersen, T. T. Alkeskjold, F. Poli, E. Coscelli, M. M. Jørgensen, M. Laurila, J. Lægsgaard and J. Broeng, "Hybrid Ytterbium-doped large-mode-area photonic crystal fiber amplifier for long wavelengths," Opt. Express **20**(6), 6010–6020 (2012).
6. COMSOL Multiphysics, "COMSOL homepage," version 4.3, www.comsol.com.
7. NKT Photonics, "LMA-25 specification sheet," first edition, 2006,www.nktphotonics.com/files/files/LMA-25.pdf.
8. J. Hansryd and P. A. Andrekson, "Fiber-Based Optical Parametric Amplifiers and Their Applications," IEEE J. Sel. Top. Quantum Electron. **8**(3), 506–520 (2002).
9. G. P. Agrawal, *Nonlinear Fiber Optics*, 4th ed. (Elsevier, United States of America, Fourth edition, 2007).
10. N. M. Litchinitser, S. C. Dunn, B. Usner, B. J. Eggleton, T. P. White, R. C. McPhedran and C. M. de Sterke, "Resonances in microstructured optical waveguides," Opt. Express **11**(10), 1243–1251 (2003).

1. Introduction

Rare earth ions are widely used as gain material in active fibers for lasers or amplifiers. The output wavelengths of active fibers are restricted by the emission cross section of the ions, and

#187876 - $15.00 USD Received 4 Apr 2013; revised 3 Jun 2013; accepted 6 Jul 2013; published 22 Jul 2013

the maximum gain is normally located at the maximum of the emission cross section. Therefore, rare earth ions might not be well-suited as gain material for all wavelengths, but other means must be considered. One approach is to utilize the nonlinear response of silica, to convert light from wavelengths easily obtained with rare earth doped gain media. For this purpose Raman scattering has been extensively investigated, however the generated light is restricted by the Raman response of silica, and the process may not be suited for all applications. Four wave mixing (FWM) allows conversion to any wavelength with a careful fiber design, and is therefore a very attractive alternative.

Group velocity dispersion (GVD) management is the key to control the products of a FWM process. The photonic crystal fiber (PCF) technology allows tailoring of the GVD profile, since the zero GVD wavelength (ZDW) can be controlled through the core size [1]. For power scaling, large mode area (LMA) fibers are required, and core scaling is not compatible with control of the ZDW in standard PCFs since material dispersion dominates. FWM in LMA PCFs has been investigated, but the spectral positions of the FWM products cannot be controlled independently of pump wavelength [2]. One way to achieve spectral control of the FWM products in LMA fibers is to utilize, that the ZDW scales with fiber mode order and perform FWM in a suitable higher order mode (HOM) in a LMA HOM fiber. With this approach FWM products in the 1 µm wavelength range has been achieved in a HOM of area 618 µm^2 [3]. However, a compromise with beam quality has to be made with this method.

In this work, FWM in a single mode (SM) LMA hybrid PCF is considered. Both airholes and high-index inclusions are present in the cladding of the hybrid PCF, combining index- and photonic bandgap (PBG) guidance. The high-index inclusions give rise to large values of normal and anomalous GVD near the edges of a transmission band, enabling control of the ZDW position and the GVD profile. This control can be utilized in the FWM process to determine the spectral position of the FWM products. Thereby it is possible to extend the wavelength coverage of high power fiber sources of high beam quality to wavelengths which may not be accessible by rare earth ions.

2. Considered fibers

2.1. Large mode area hybrid photonic crystal fibers

In Fig. 1(a) a microscope image of a SM LMA hybrid PCF is shown. The fiber is a double-clad silica PCF, with an airclad as the outer cladding. The inner cladding consists of airholes with diameter 1.5 μm placed in a hexagonal lattice and hole-to-hole spacing $\Lambda = 9.9\,\mu$m. Seven missing airholes define the core. One row of airholes has been replaced with high-index Germanium-doped silica rods (Ge-rods) with numerical aperture (NA) 0.29. The diameter of the Ge-rods on one side of the core (the left side in Fig. 1(a)), d_{small}, is reduced with respect to the diameter of the Ge-rods on the other side of the core, d_{large}, resulting in a asymmetric design. The sizes are $d_{\text{small}} = 6.0\,\mu$m and $d_{\text{large}} = 7.1\,\mu$m.

The Ge-rods give rise to a PBG effect, thereby combining two guiding mechanisms in the hybrid PCF. Light in the core is confined by index guiding, due to the airholes, and by PBG guiding, due to the Ge-rods. By adjusting the airhole diameter, the fiber can be made SM for large core sizes, and the PBG guiding introduces a built-in spectral filter. The asymmetric design gives rise to two different sets of cladding modes, one for the small and one for the large Ge-rods. Thereby it is possible to adjust the transmission windows of the fiber both from the blue- and red edge [4, 5].

In Fig. 2(a) a white light transmission measurement of the hybrid PCF is shown. White light from a Halogen-Tungsten Lamp is launched in a 7 m long fiber coiled with 4 turns to diameter ~ 45 cm. The fiber is coiled in a plane parallel to the axis of the Ge-rods, and with the small Ge-rods on the outside of the bend with respect to coil center. A fiber with core diameter

#187876 - $15.00 USD Received 4 Apr 2013; revised 3 Jun 2013; accepted 6 Jul 2013; published 22 Jul 2013

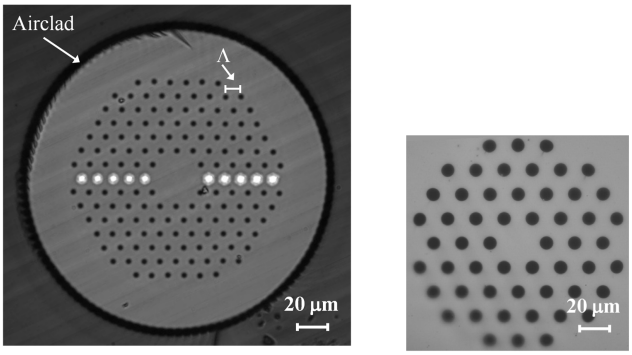

Fig. 1. Microscope images of the considered fibers. (a) A silica double-clad large mode area hybrid photonic crystal fiber, with an airclad as the outer cladding. The inner cladding consists of airholes (black circles) placed in a hexagonal lattice with hole-to-hole spacing Λ and seven missing airholes define the core region. One row of airholes is replaced with high-index Germanium-doped silica rods of two sizes (white circles), one on each side of the core, respectively. (b) A silica large mode area photonic crystal fiber. Airholes (black circles) are placed in a hexagonal lattice, and a single missing airhole defines the core region.

20 μm and NA$\sim$ 0.6 is butt-coupled to the core at the output end of the PCF, thereby spatially filtering out cladding light. Two transmission bands are observed, one with a spectral position of 1040 nm – 1080 nm, and one placed at 1120 nm – 1165 nm.

In Fig. 2(b) the calculated overlap integral of the Fundamental Mode (FM) polarized along the Ge-rods with the core region is shown. The overlap integral has been calculated with a full-vector modal solver based on the finite element method [6]. The same dimensions as for the fabricated PCF are used in the calculations. For overlap integral values approaching 1, the core mode is well confined, and the spectral region can be interpreted as a transmission band. In Fig. 2(b) the transmission bands are observed at 990 nm – 1070 nm and 1095 nm – 1112 nm. The discrepancies with the measured transmission bands can be caused by uncertainties in the actual values of parameters for the fabricated fiber, such as refractive indices and sizes of Ge-rods.

In Fig. 2(c) the calculated GVD parameter, D, of the spectrally broadest transmission band is shown. The ZDW is positioned at 1054.5 nm, shorter wavelengths lie in the normal dispersion regime, while the dispersion is anomalous for longer wavelengths. Near the bandedges the curve grows substantially. The presence of resonant coupling with the Ge-rods, thus gives rise to large normal and anomalous dispersion values on the bandedges.

2.2. Large mode area photonic crystal fiber

A commercially available 7 m long 25 μm core SM LMA PCF (LMA-25) is considered as a reference fiber [7]. The purpose of this fiber is to illustrate the output of a PCF with similar mode area, but without any resonant cladding elements. In Fig. 1(b) a microscope image of the fiber is shown, the ratio between airhole diameter and hole-to-hole spacing is 0.48, and one missing airhole defines the core region. In Fig. 2(d) the calculated D, is shown. The ZDW of this fiber is positioned at 1253.5 nm and FWM is expected to occur for pump wavelengths in the vicinity of the ZDW. In this work a pump wavelength of 1064 nm is considered, and thus Raman scattering is expected to be the dominant nonlinear effect instead.

#187876 - $15.00 USD Received 4 Apr 2013; revised 3 Jun 2013; accepted 6 Jul 2013; published 22 Jul 2013

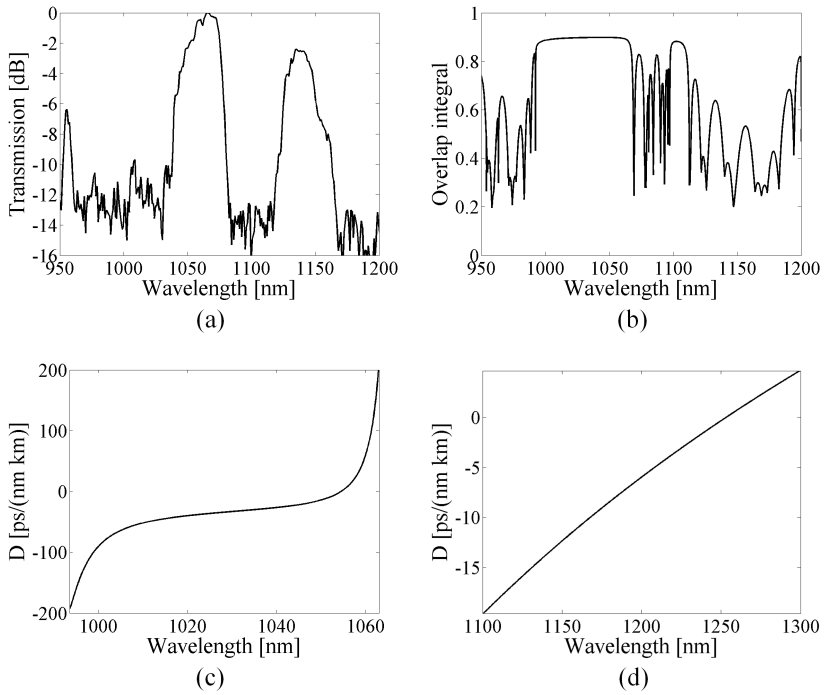

Fig. 2. (a) White light transmission measurement of the hybrid photonic crystal fiber. (b) Calculated overlap integral of the fundamental mode in the hybrid photonic crystal fiber polarised along the Germanium-doped silica rods with the core region. (c) Calculated group velocity dispersion parameter in the transmission band 995 nm – 1065 nm of Fig. 2(b). (d) Calculated group velocity dispersion parameter of a large mode area photonic crystal fiber without high-index inclusions in the cladding.

3. Four wave mixing

FWM is a third order nonlinear effect, involving four frequency components; ω_{p1}, ω_{p2}, ω_s, and ω_i. ω_{p1} and ω_{p2} are the pump photons, which are annihilated in the process, and ω_s and ω_i are the signal and idler photon, respectively, which are created in the process. In this work degenerate FWM is considered, thus only one pump is considered $\omega_{p1} = \omega_{p2} = \omega_p$. Energy conservation must be fulfilled, the requirement is given by $2\omega_p = \omega_s + \omega_i$. For the process to occur efficiently, the phase mismatch should be as small as possible. The contribution to the phase mismatch arising from the linear dispersion is given by $\Delta\beta = \beta(\omega_s) + \beta(\omega_i) - 2\beta(\omega_p)$, where $\beta(\omega_s)$, $\beta(\omega_i)$, and $\beta(\omega_p)$ is the propagation constant at signal, idler, and pump frequency, respectively. There is also a nonlinear contribution to the phase mismatch due to the Kerr effect. Both contributions are taken into account in the following calculations of the parametric gain.

3.1. Parametric gain

The parametric gain is calculated from three coupled differential equations describing the dynamics of the pump power, signal power, and idler power [8]. The single pass gain is given by $\mathrm{P_s}(L)/\mathrm{P_s}(0)$, where $\mathrm{P_s}(L)$ is the output signal power after a fiber length L, and $\mathrm{P_s}(0)$ is the input signal power. In this work spontaneous degenerate FWM is considered, meaning that the generated signal and idler components build up from noise. The signal input power is set to

#187876 - $15.00 USD Received 4 Apr 2013; revised 3 Jun 2013; accepted 6 Jul 2013; published 22 Jul 2013

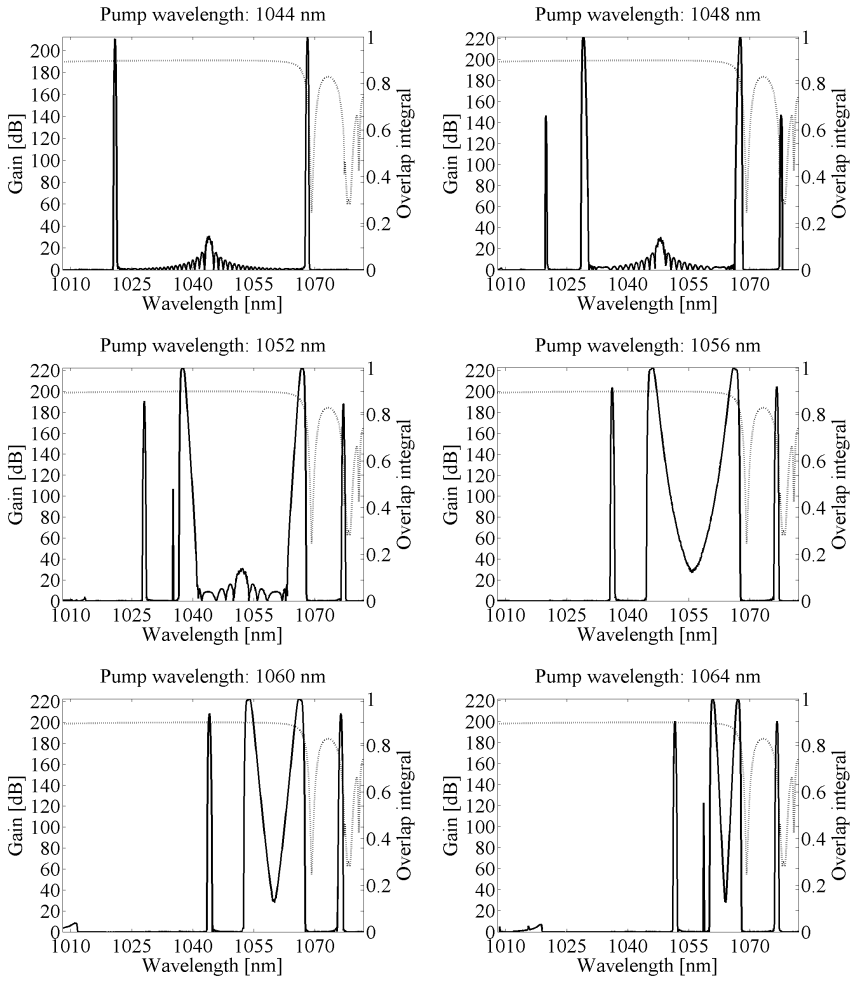

Fig. 3. Calculated parametric gain for different pump wavelengths. The solid line is the parametric gain (y-axis on the left), the dashed line is the overlap integral (y-axis on the right). The pump wavelengths 1044 nm, 1048 nm, and 1052 nm lie in the normal dispersion regime, 1056 nm, 1060 nm, and 1064 nm in the anomalous dispersion regime, with zero dispersion wavelength at 1054.5 nm.

the energy of one photon at 1064 nm per second, giving $1.9 \times 10^{-19}\ \frac{\mathrm{J}}{\mathrm{s}}$. Parametric gain in this context thus describes gain of quantum noise.

The interacting pump, signal and idler fields must overlap spatially. In PCF's, as the LMA-25, this is approximately fulfilled, and the calculations can be simplified by replacing field overlap integrals with a term including the effective mode area. In a hybrid PCF, where resonant coupling occurs, these overlaps can vary significantly, and the field overlap integrals must be taken into account [9]. The pump propagates in the FM of the hybrid PCF. The largest field overlap with signal and idler is thus expected, if the signal and idler are also generated in the FM. The FM has therefore been chosen as the relevant field in all calculations.

In Fig. 3 the calculated parametric gain with 0.1 nm resolution for a pump peak power of 10 kW, and for pump wavelengths 1044 nm, 1048 nm, 1052 nm, 1056 nm, 1060 nm, and

#187876 - $15.00 USD Received 4 Apr 2013; revised 3 Jun 2013; accepted 6 Jul 2013; published 22 Jul 2013

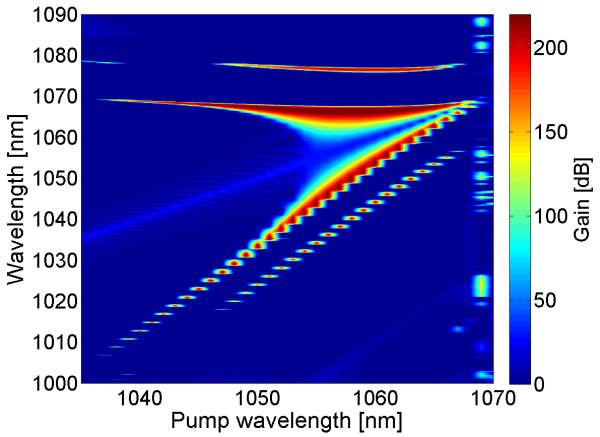

Fig. 4. Surface plot of the parametric gain for pump wavelengths 1035 nm to 1070 nm in steps of 1 nm.

1064 nm, is shown (solid line). Furthermore the overlap integral is plotted (dashed line) to illustrate the positions of the gain peaks with respect to the transmission bandedges.

The pump wavelength 1044 nm lies in the normal dispersion regime, and $\sim$ 10 nm away from the ZDW of 1054.5 nm. For this pump wavelength a very narrow gain line is observed at the bandedge of 1068 nm corresponding to the Stokes wave. The anti-Stokes wave lies within the transmission band. For pump wavelengths approaching ZDW the gain bandwidth of the Stokes and anti-Stokes wave increases, and the anti-Stokes wave redshifts spectrally. Furthermore a second set of Stokes and anti-Stokes waves is observed, caused by a resonance near 1076 nm. For pump wavelength 1056 nm two gain peaks at 1046 nm and 1066 nm with Full Width at Half Maximum (FWHM) of 1.2 nm, and two narrow gain peaks at 1036 nm and 1077 nm with FWHM of 0.1 nm, are observed. For pump wavelengths further redshifted from the ZDW, the gain peaks narrow. Furthermore a very narrow peak is observed for pump wavelengths 1052 nm and 1064 nm at 1035 nm and 1059 nm. These are probably artefacts of the resolution of the calculation.

Gain at the Stokes wave at the 1068 nm bandedge is observed for a large range of the considered pump wavelengths, with a spectral position within 1067 nm-1069 nm. The gain peak of the anti-Stokes wave lies within the transmission band and redshifts with increasing pump wavelengths. This behaviour is clarified in Fig. 4, where a surface plot of the gain versus pump wavelength is shown.

In Fig. 4 gain of a Stokes wave near 1068 nm is observed for all pump wavelengths, the peak position varies between 1066 nm and 1069 nm. The gain peak of the anti-Stokes wave within the transmission band redshifts with increasing pump wavelengths. Gain at a Stokes wave near 1076 nm is also observed, with the anti-Stokes wave lying in the transmission band, and redshifting with increasing pump wavelength. The 1076 nm Stokes wave is caused by resonant coupling at this wavelength.

The dispersion profile grows rapidly near a bandedge and flattens inside the transmission band. This behaviour allows phasematching within a wavelength range of a few nanometres, even for a large range of pump wavelengths. The spectral position of the parametric gain can therefore be controlled by the Ge-rod sizes in the fiber. The FWM product at the bandedge will be resonant with cladding modes and thus leak out of the core. However, the FWM product

#187876 - $15.00 USD Received 4 Apr 2013; revised 3 Jun 2013; accepted 6 Jul 2013; published 22 Jul 2013

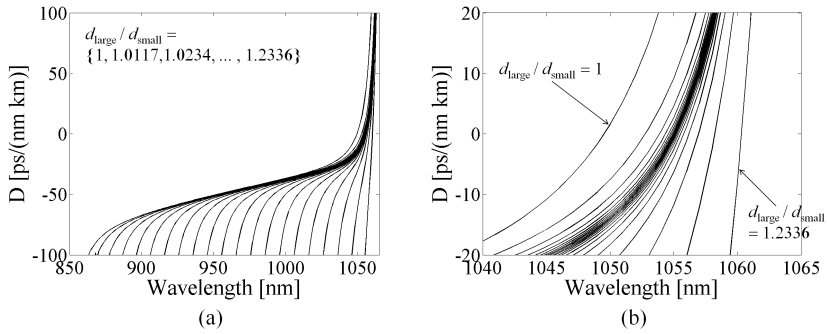

Fig. 5. (a) Group velocity dispersion profiles in the transmission band for the hybrid photonic crystal fiber for a range of $d_{\text{large}}/d_{\text{small}} = 1, ..., 1.2336$ in step sizes of 0.0117. (b) Zoom of the group velocity dispersion profiles near the zero dispersion wavelength.

within the transmission band is expected to be well-confined with a LMA. FWM to the mode within the transmission band thus allows for power scaling of the process.

In practice the narrow gain peaks observed in Fig. 3 can be quite hard to utilize, since small fluctuations in the fabricated fiber structure along the propagation length, can be detrimental for the phasematching requirement. Size differences in the Ge-rods along the fiber length will alter the resonant conditions slightly, and thus shift the spectral position of the parametric gain peak. As a consequence a broader gain of lower magnitude is expected in practice, when pumping far away from the ZDW, and a compromise between increasing the fiber length, to obtain a longer nonlinear length and increase the FWM interaction, and the limitation of fabricating a long fiber without structural fluctuations can arise.

3.2. Tailoring the dispersion profile

The spectral width of the gain peaks can be increased by tailoring of the ZDW. The spectral position of the ZDW can be adjusted, by adjustment of the spectral position of the bandedges, controlled through the Ge-rod sizes. In Fig. 5(a) a calculation of D is seen for different values of d_{large}, while d_{small}, is kept constant at $6\,\mu$m. The ratio $d_{\text{large}}/d_{\text{small}}$ is varied from 1 to 1.2336 in steps of 0.0117, also stated in Fig. 5(a). In Fig. 5(b) a zoom near the ZDW is seen. By altering d_{large} it is possible to tune ZDW in a range of 10 nm. However, the slope of the dispersion profile at the bandedges also changes and thus the phasematching condition. In the following a pump wavelength of 1056 nm will be considered for two different scenarios; one with the pump positioned in the normal and anomalous dispersion regime for $d_{\text{large}}/d_{\text{small}}$ having the values 1.2336 and 1, respectively. The scenarios are illustrated in Fig. 6.

In Fig. 7(a) and Fig. 7(b) calculated parametric gain curves (solid lines) with 0.1 nm resolution for a pump wavelength of 1056 nm and pump peak power of 8 kW are shown for two different ratios of $d_{\text{large}}/d_{\text{small}}$, 1 and 1.2336, respectively. Furthermore the overlap integral is plotted (dashed line) to illustrate the positions of the gain peaks with respect to the transmission bandedges. For $d_{\text{large}}/d_{\text{small}} = 1$ the pump wavelength lies in the anomalous dispersion regime with $\text{D} = 51\,\text{ps/(nm km)}$, and for $d_{\text{large}}/d_{\text{small}} = 1.2336$ the pump wavelength lies in the normal dispersion regime with $\text{D} = -65\,\text{ps/(nm km)}$. By further redshifting the blue edge of the transmission band to a point where the blue edge is closer spaced in frequency to the pump wavelength than the red edge, a gain peak at the blue edge would be observed instead.

From Fig. 7(a) and Fig. 7(b) it is clearly demonstrated that the dispersion profile can be

#187876 - $15.00 USD Received 4 Apr 2013; revised 3 Jun 2013; accepted 6 Jul 2013; published 22 Jul 2013

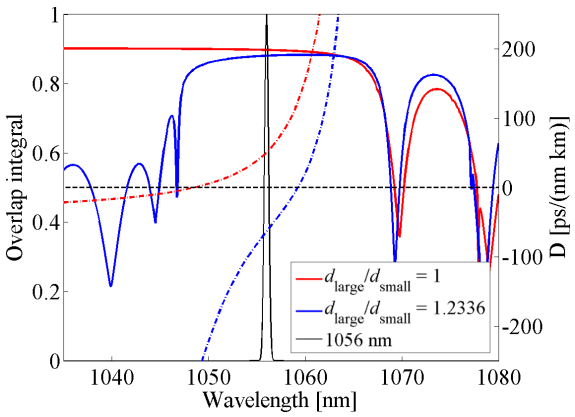

Fig. 6. Overlap integrals (solid lines, y-axis on the left) and group velocity dispersion parameters (dashed lines, y-axis on the right) for the two ratios $d_{\text{large}}/d_{\text{small}} = 1$ and $d_{\text{large}}/d_{\text{small}} = 1.2336$. Furthermore a Gaussian distribution is plotted at 1056 nm to mark the pump wavelength. For the $d_{\text{large}}/d_{\text{small}} = 1$ the pump is located in the anomalous dispersion regime and for $d_{\text{large}}/d_{\text{small}} = 1.2336$ the pump is located in the normal dispersion regime.

tailored to obtain a broader gain peak. Furthermore, the signal wavelength is better confined in the transmission band for $d_{\text{large}}/d_{\text{small}} = 1$ than for $d_{\text{large}}/d_{\text{small}} = 1.2336$. Larger overlap integrals of signal, idler and pump fields are therefore obtained for $d_{\text{large}}/d_{\text{small}} = 1$, leading to an increase in maximum gain. However, the maximum gain is positioned at 1063.5 nm and 1068.9 nm for $d_{\text{large}}/d_{\text{small}} = 1$ and $d_{\text{large}}/d_{\text{small}} = 1.2336$, respectively. The tailoring thus also has an impact on the maximum gain position.

In Fig. 7(c) the parametric gain has been calculated for the ratio $d_{\text{large}}/d_{\text{small}} = 1$, but now the diameter of the small Ge-rods is increased with 0.1 μm, to shift the spectral position of the maximum gain. In this case, the maximum gain is positioned at 1068.9 nm. The pump wavelength is still located in the anomalous dispersion regime with D = 8 ps/(nm km). It is therefore possible to maintain pump wavelength and spectral position of the maximum gain, but broaden the gain peak by tailoring the dispersion profile through the Ge-rod sizes.

4. Experimental results

4.1. Measurement setup

A schematic illustration of the measurement setup is shown in Fig. 8. A 40 ps 1064 nm laser with a repetition rate of 1 MHz and a linear polarized output is used for the measurements. The laser average output power is kept constant at 4.5 W through out the measurements, and a half-wave plate ($\frac{\lambda}{2}$) and Polarizing Beamsplitter Cube (PBC) are inserted to adjust the power launched in the fiber. The half-wave plate following the PBC is inserted to ensure the laser is polarized along the axis of the Ge-rods in the PCF. Furthermore a 1064 nm laser line filter is inserted to remove any amplified spontaneous emission from the laser.

The laser is launched in a 7 m long PCF coiled with four turns to diameter (D_{coil}) ~45 cm. The output of the PCF is imaged onto a pick-up fiber with core diameter 5 μm and NA ~ 0.6 through a glass wedge. The pick-up fiber is connected to an Optical Spectrum Analyzer (OSA).

The image size of the airclad of the PCF at the position of the pick-up fiber is approximately 15 mm in diameter, thus the pick-up fiber will only collect light from a small segment of the

#187876 - $15.00 USD Received 4 Apr 2013; revised 3 Jun 2013; accepted 6 Jul 2013; published 22 Jul 2013

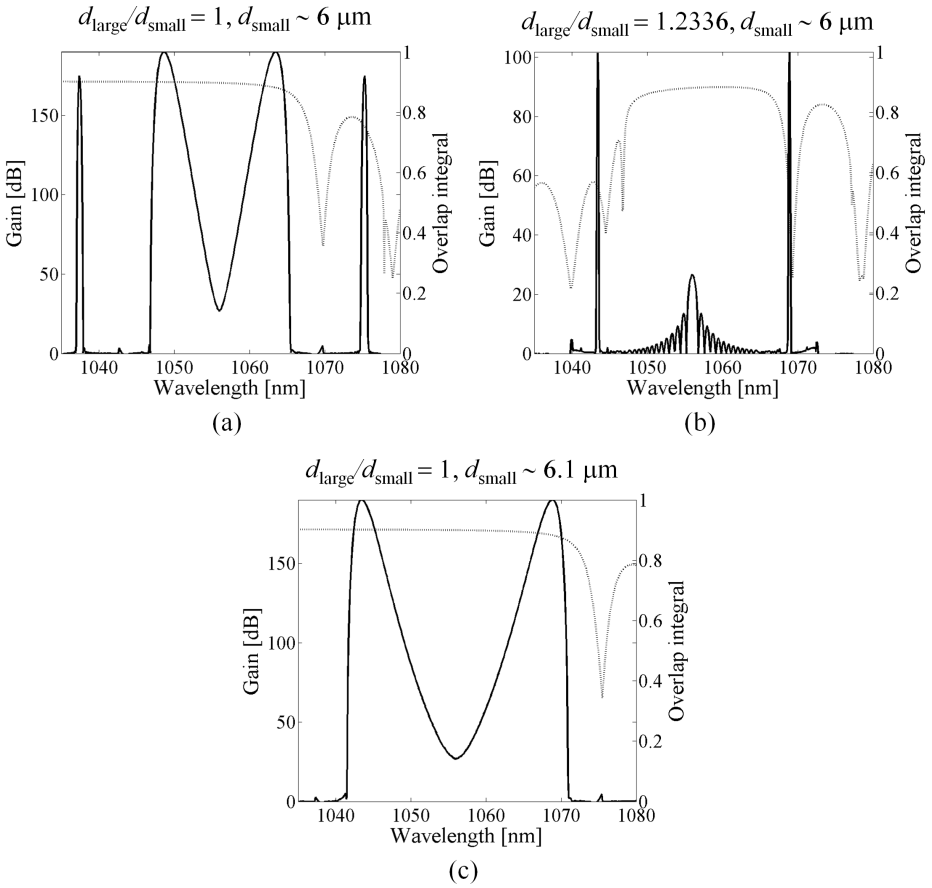

Fig. 7. Calculated parametric gain (solid line, y-axis on the left) for a pump wavelength of 1056 nm. The overlap integral is also shown (dashed line, y-axis on the right), to illustrate the position of the gain with respect to the transmission band. (a) Pump wavelength is positioned in the anomalous dispersion regime, $d_{large}/d_{small} = 1$, $d_{small} = 6.0\,\mu$m. (b) Pump wavelength is positioned in the normal dispersion regime, $d_{large}/d_{small} = 1.2336$, $d_{small} = 6.0\,\mu$m. (c) Pump wavelength is positioned in the anomalous dispersion regime, $d_{large}/d_{small} = 1$, $d_{small} = 6.1\,\mu$m.

#187876 - $15.00 USD Received 4 Apr 2013; revised 3 Jun 2013; accepted 6 Jul 2013; published 22 Jul 2013

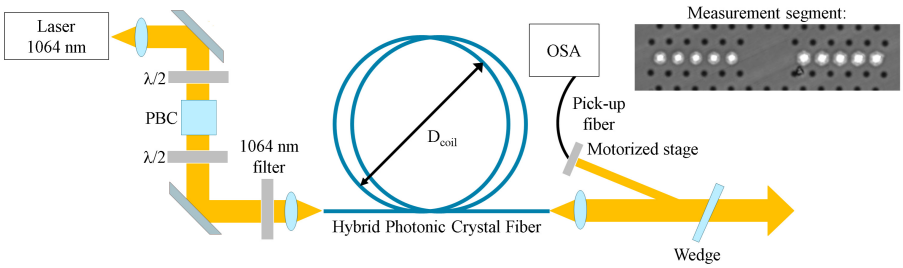

Fig. 8. Schematic illustration of the experimental setup. The linear polarized laser light is launched in the hybrid photonic crystal fiber through a half-wave plate ($\frac{\lambda}{2}$) and a Polarizing Beamsplitter Cube (PBC), followed by a second half-wave plate ($\frac{\lambda}{2}$). A 1064 nm laser line filter of FWHM $\sim$ 4 nm is inserted to clean-up the laser light. The fiber output is imaged onto a pick-up fiber with core diameter 5 μm and NA $\sim$ 0.6 through a glass wedge. The pick-up fiber is connected to an Optical Spectrum Analyzer (OSA). The measured fiber segment is also shown.

PCF. The pick-up fiber is placed on a motorized stage, such that a large segment of the PCF output can be measured step-by-step. The measured segment of the PCF is shown in Fig. 8. In total width $\times$ height $= 211 \times 51 = 10761$ measurements have been performed for this segment for each considered input power. This results in a spatially and spectrally resolved image of the PCF output, with the spatial resolution decided by the pick-up fiber core diameter, and image size of the PCF output at the pick-up fiber position.

The LMA-25 fiber was measured with the same setup, however in this case, the pick-up fiber was placed at core center for all measurements.

4.2. Core spectra

In Fig. 9(a) the output power of the LMA-25 fiber for different pump powers is shown. Raman scattering is observed near 1118 nm for peak powers above approximately 35 kW. Furthermore self-phase modulation (SPM) is observed as sidebands in the vicinity of the pump wavelength.

In Fig. 9(b) the output power from the hybrid PCF core for different pump powers is shown. In these measurements the pick-up fiber is positioned at core center, similar to the measurements presented in Fig. 9(a). Furthermore the white light transmission measurement is plotted to illustrate the output with respect to transmission bandedges. The bandeedges are also indicated with white dashed lines in the figure. For pump peak powers above approximately 60 kW spectral components at 1083 nm and 1045 nm build up, caused by FWM. SPM is also observed, however, the shape of the transmission band clearly imprints on the output spectrum, and the SPM peak on the red side of the pump is the most evident in the figure. The SPM peak on the blue side of the pump experiences a larger loss, and the collected power is thus lower.

There is a clear difference between the output of the LMA-25 fiber and the hybrid PCF. No FWM is observed in the LMA-25, instead Raman scattering is the dominant nonlinear effect, and no Raman scattering is observed in the hybrid PCF, instead FWM becomes the dominant nonlinear effect. The spectral position of the maximum Raman gain falls outside the transmission band in the hybrid PCF, which could also explain why Raman scattering is not observed for this fiber.

#187876 - $15.00 USD Received 4 Apr 2013; revised 3 Jun 2013; accepted 6 Jul 2013; published 22 Jul 2013

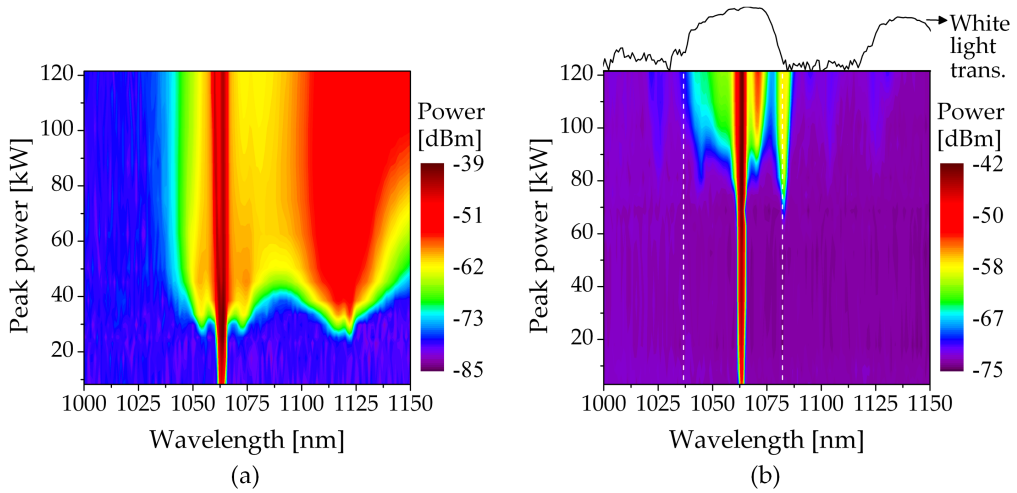

Fig. 9. (a) Output power of a large mode area photonic crystal fiber (LMA-25) for a range of input pump peak powers. Raman scattering is observed above 1100 nm, and self-phase modulation is observed in the vicinity of the pump. (b) Core output power of a hybrid large mode area photonic crystal fiber for a range of input pump peak powers. Furthermore the white light transmission spectrum of Fig. 2(a) is plotted. Self-phase modulation and four wave mixing is observed.

4.3. Spectral power distribution

In Fig. 10 output powers from the full measured PCF segment are shown for different launched laser powers. The figures are obtained by integration of all the measured spectra, one from each measurement point. For a peak power of 56.5 kW FWM is observed at 1045 nm and 1083 nm, the latter located at the red edge of the transmission band. For peak powers of 66.5 kW and above additional FWM products are observed at 1023 nm and 1104 nm. Considering Fig. 2(a), a dip in the white light transmission spectrum is observed at 1030 nm, indicating a resonant coupling at this wavelength. This resonance could give rise to the FWM products at 1023 nm and 1104 nm. The peaks could however also be caused by cascaded FWM, since their spectral positions matches the first FWM sidebands.

The measured power at 1083 nm is significantly higher than at 1045 nm. Only a segment of the PCF output has been measured, so a fraction of the power at 1045 nm could be located outside the considered area. For an input peak power of 102.5 kW 19 % of the measured power is located at the 1083 nm peak. However, a measurement of a segment of the PCF including the full airclad is needed to clarify the conversion efficiency of the total output power.

By matching a simulation to the measured transmission spectrum, such that the calculated transmission bandedges matches the measured transmission bandedges, the GVD parameter at the laser wavelength can be estimated. From such a consideration a value of $D = -10$ ps/(nm km) is calculated. This indicates the pump is positioned in the normal dispersion regime, and thus narrow FWM lines are expected, which agrees reasonably with the measured output spectra. However, only the transmission bandedges are matched in the calculations, not the shape of the measured transmission band, so the actual GVD parameter may be slightly different than the calculated.

#187876 - $15.00 USD Received 4 Apr 2013; revised 3 Jun 2013; accepted 6 Jul 2013; published 22 Jul 2013

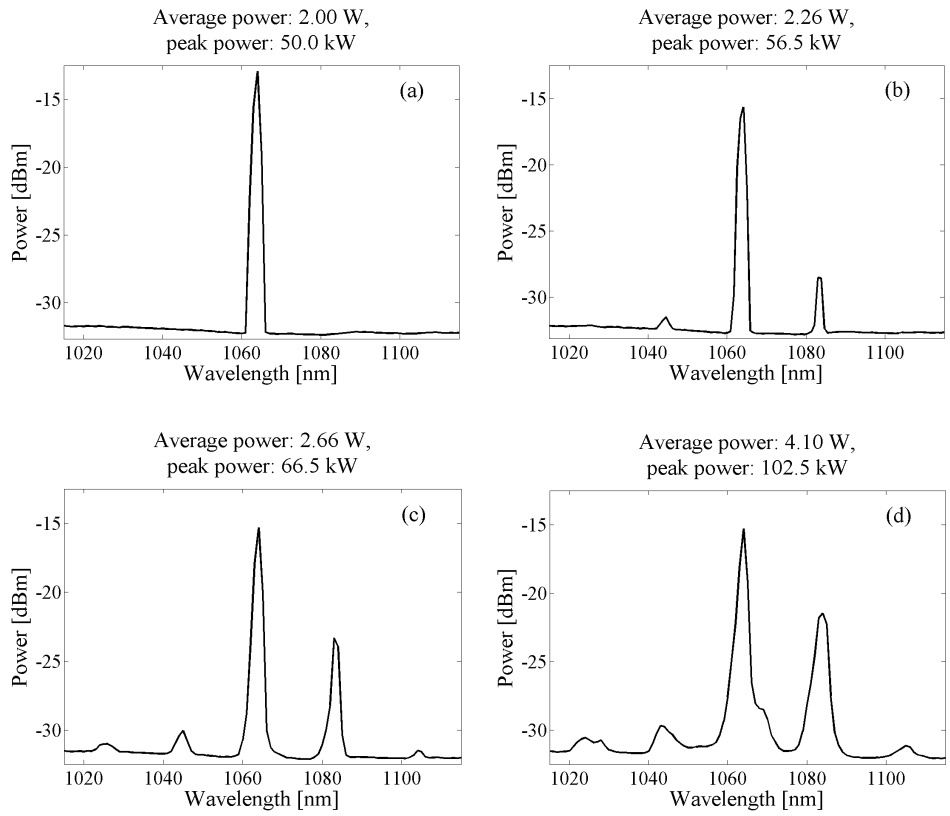

Fig. 10. Output power of the hybrid photonic crystal fiber, the input average power and peak power are given in the titles. Four wave mixing is observed for increasing launched laser power

4.4. Spatial power distribution

In Fig. 11(a) the spatial power distribution at wavelengths 1023 nm, 1045 nm, 1064 nm, 1083 nm, and 1104 nm are shown for an input peak power of 102.5 kW. In all plots the values are normalized to the maximum power value at that given wavelength, which is also stated in the plots. The clarity of the PCF structure depends on how well the output is focused in the plane of the pick-up fiber end facet. In these measurements the modes of the Ge-rods are clearly distinguishable, indicating a reasonable focus.

It is clearly seen, that the maximum intensity is located at different positions for different wavelengths. At 1023 nm the maximum intensity is located in the first Ge-rod to the right of the core, while for 1045 nm the maximum intensity is located in the fourth Ge-rod. At 1064 nm the mode is well confined in the core region, and the maximum intensity is found at core center. For 1083 nm and 1104 nm the Ge-rods to the left of the core become resonant, and coupling to this side is observed. At 1083 nm the maximum intensity is found at the fifth and outermost Ge-rod, while the maximum intensity of 1104 nm is located in the first Ge-rod.

Calculated field distributions at 983 nm and 1081 nm are shown in Fig. 11(b) and 11(c), respectively. 983 nm is near the blue edge in the calculated transmission band and 1081 nm near the red edge. The field distributions are similar to the measured power distributions at 1045 nm

#187876 - $15.00 USD Received 4 Apr 2013; revised 3 Jun 2013; accepted 6 Jul 2013; published 22 Jul 2013

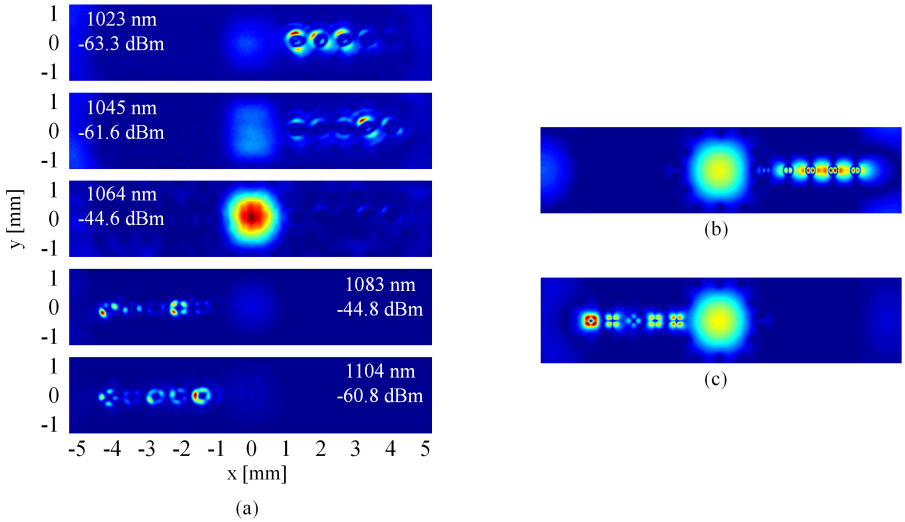

Fig. 11. (a) Spatial power distribution at wavelenghts 1023 nm, 1045 nm, 1064 nm, 1083 nm, and 1104 nm, with the power magnitude on a linear scale, for a launched laser peak power of 102.5 kW. The plots are normalized to the maximum measured power at each given wavelength, also stated in the plots. (b) Calculated spatial field distribution at 983 nm. (c) Calculated spatial field distribution at 1081 nm.

and 1083 nm, at 983 nm the maximum value of the field is located in the fourth Ge-rod on the right-hand side of the core, while at 1081 nm the maximum value of the field is located in the fifth rod on the left hand side of the core. Furthermore the LP_{12}-like modes observed in the Ge-rods at 1023 nm and 1045 nm in the measurements, are also seen in the calculated field distribution at 983 nm, and the LP_{21}-like modes observed at 1083 nm and 1104 nm in the measurements, are also seen in the calculated field distribution at 1081 nm. The modes are cut-off in the Ge-rods near these wavelengths, and thus agrees with the core mode coupling to these modes [10].

In Fig. 12 two spectra at two different measurement points are shown. Which measurement points they correspond to is marked in the inset of the graph in the upper left corner. The solid line graph corresponds to the maximum intensity point at 1064 nm, that is the core center, while the dashed line graph corresponds to the point of maximum intensity of 1083 nm, in the fifth and outermost Ge-rod. From this figure it is evident, that light at 1083 nm is generated with almost the same intensity (0.2 dB lower) as the 1064 nm output. However, this intensity is only present in a single measurement point, and as seen in Fig. 10(d) the output power at 1064 nm is larger than at 1083 nm. However, if the generated light should be used for subsequent nonlinear processes, the high intensity can be of great interest.

Both numerical and experimental results show FWM products on the edges of the transmission bands. The FWM Stokes line experimentally coincide with the red edge of the transmission band, thus coupling to the Ge-rods is observed. In order to utilize the 1083 nm light, a pick-up method has to be applied. For example a Ge-doped fiber with similar dimensions as the Ge-rod could be butt-coupled or spliced to the fifth Ge-rod on the right, see Fig. 12(a), and the light could be collected and transferred to other uses. The efficiency of collecting the light from the Ge-rod can in principal be quite high, by choosing a proper pick-up fiber with identical mode properties as the Ge-rod, and careful alignment. With this purpose in mind, the resonant coupling to the Ge-rod is an advantage, since it separates the FWM products spatially from the

#187876 - $15.00 USD Received 4 Apr 2013; revised 3 Jun 2013; accepted 6 Jul 2013; published 22 Jul 2013

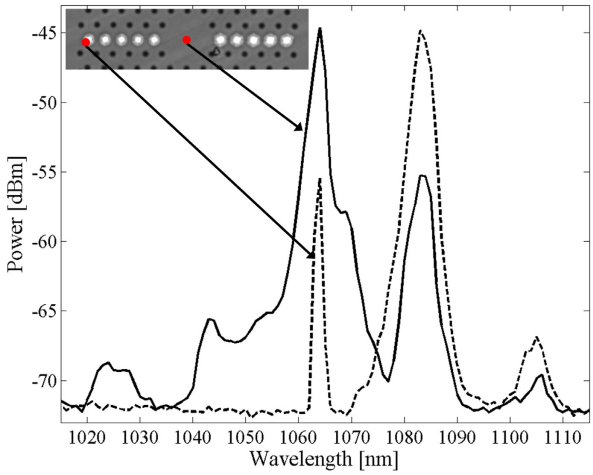

Fig. 12. Spectra from selected measurement points. The spectra correspond to the measurements where the pick-up fiber is positioned at the largest power output point for 1064 nm and 1083 nm, respectively. These positions are marked in the inset.

laser wavelength, and thus no filters are needed to extract the FWM products, only a simple butt-coupling or splicing. However, the mode area is restricted by the Ge-rod size, and furthermore the light is coupling to HOMs. Instead, the anti-stokes component within the transmission band is of interest, to maintain the LMA SM properties. The shape of the transmission band is clearly seen imprinted on the spectrum in Fig. 9(b), and at 1045 nm there is a loss of 4 dB in the fiber of length 7 m with respect to maximum transmission. Thus the anti-stokes FWM component also couples out of the core. The blue edge of the transmission band could be blue shifted by decreasing the size difference between d_{small} and d_{large} to confine the 1045 nm component and achieve FWM in a large area mode with SM properties. Considering a signal experiencing gain at the anti-Stokes component, the idler will be generated at the Stokes line on the bandedge, and thus couple out of the core leading to a loss. This loss will prevent the signal and idler to back-convert to the pump frequency. The build-in spectral filtering of the idler can thus potentially increase the conversion efficiency from pump to signal [2].

5. Conclusion

In this work spontaneous degenerate FWM in LMA hybrid PCFs was considered numerically and experimentally. The transmission bands of such fibers can be adjusted both from the blue- and red edge, thus giving great control of the transmission properties. The GVD grows substantially at an edge of a transmission band, giving large normal dispersion on the blue edge, and large anomalous dispersion on the red edge. The dispersion profile can thus be controlled in a LMA hybrid PCF by adjustment of the transmission bands.

Numerically it was found that parametric gain was achieved on a bandedge for a large range of pump wavelengths. Experimentally FWM products were also observed on bandedges. The hybrid PCF therefore provides spectral control of the FWM products. By proper fiber design, a FWM product can be generated within the transmission band, thereby obtaining FWM in a large area mode with SM properties. FWM in hybrid PCFs therefore provides the possibility to extend the wavelength coverage of high power fiber sources.

#187876 - $15.00 USD Received 4 Apr 2013; revised 3 Jun 2013; accepted 6 Jul 2013; published 22 Jul 2013